Intermittency and bifurcation in SEPICs under voltage-mode control*

Liu Fang(刘 芳)†

College of Electrical and Information Engineering, North China University for Nationalities, Yinchuan 750021*, China*

(Received 22 April 2009; revised manuscript received 5 March 2010)

A stroboscopic map for voltage-controlled single ended primary inductor converter (SEPIC) with pulse width modulation (PWM) is presented, where low-frequency oscillating phenomena such as quasi-periodic and intermittent quasi-periodic bifurcations occurring in the system are captured by numerical and experimental methods. According to bifurcation diagrams and nonlinear dynamical theory, the characteristics of the low-frequency oscillation and the mechanism for the appearance of the low-frequency oscillation are investigated. It is shown that as the controller parameter varies, the change in the conduction mode takes place from the continuous conduction mode (CCM) under the originally stable period one and high periodic orbits to the intermittent changes between CCM and discontinuous conduction mode (DCM), which may be related to the losing stability of the system and brought the system to exhibiting low-frequency oscillating behaviour in the time domain. Moreover, the occurrence of the intermittent quasi-periodic oscillation reflects that the system undergoes a Neimark–Sacker bifurcation.

Keywords: low-frequency oscillation, intermittency, single ended primary inductor converter, Neimark–Sacker bifurcation

PACC: 0545

1. Introduction

During the past two decades, nonlinear dynamics occurring in low-order converters including Buck, Boost and Buck–Boost, have been widely reported.[1−8] It is well known that such systems may exhibit high- or low-frequency nonlinear phenomena such as period-doubling bifurcation, quasi-periodicity, fractal basins of attraction[9] and chaos, etc. In this field of research, the more relevant contributions are due to Hamill and Deane. They first examined first and second-order voltage-mode controlled pulse width modulated Buck converters and current-programmed Boost converter. By means of numerical and experimental methods, the converters have been shown to bifurcate from a stable state to high-frequency subharmonic oscillations, then to chaos.[10−12] Later, low-frequency instabilities, such as Neimark–Sacker bifurcation and two-dimensional (2D) torus breakdown have been shown to occur in a pulse width modulation (PWM) voltage-controlled Boost and Buck converters, respectively.[13,14] The occurrence of such irregular phenomena may lead to high amplitude electromagnetic noise, sudden collapse in output voltage, and feedback oscillation, etc., which will degrade the system performance.[15] Henceforth, people have recognized that the research of such irregular behaviours can motivate requirement for a deeper understanding of the corresponding dynamical behaviours and further exploration of some new operation modes.

More recently, much attention has been given to SEPIC topology because it has several unique characteristics[16−18] which make it suitable for applications requiring a wide output voltage range. As is common to all power electronic systems, SEPIC is a high-order strongly nonlinear system, and may exhibit a great variety of irregular behaviours with improper choice of system parameters. So, associated bifurcations in SEPICs must be deeply studied so as to find the proper parameter space to guarantee the stability of their performance. Reference [19] showed the route to chaos via period-doubling in the SEPIC, which is designed to operate in continuous conduction mode (CCM) and under peak-current-programmed control, by means of a discrete-time model. With a stroboscopic map, Liu *et al.* captured the bifurcation phenomena, such as period-doubling, border-collision and coexistence of different attractors, occurring in a current-programmed SEPIC under CCM.[20] Based on the theory of the variable structure system, Wang

*Project supported by the Natural Science Foundation of Ningxia Autonomous Region, China (Grant No. NZ0954).

†Corresponding author. E-mail: fangliu214@163.com

© 2010 Chinese Physical Society and IOP Publishing Ltd

et al. examined the low-frequency instabilities of an SEPIC with sliding control mode and confirmed the existence of nonlinear phenomena, i.e., double limit cycle, quasi-periodicity, and chaos.[21] Being a higher order nonautonomous system, we recognize that the voltage-controlled SEPIC, which is widely used in industrial applications, may exhibit more complicated nonlinear phenomena. Unfortunately, very few have ever attempted to properly analyse the nonlinear phenomena of the circuit system as yet.

It is well known that a proper model and an analytical method are critical to the study on bifurcations and stabilities in DC–DC converters. In fact, a lot of effort has been made for studying the stability of the circuits from different points of view (see Refs. [22] and [23], and the references therein). By now, the most popular continuous technique is the small-signal analysis.[24,25] However, this modeling technique fails to predict high-frequency nonlinear phenomena due to the switching behaviour of the regulator. Being a multi-structural system operating cyclically in time, the discrete time modeling approach seems to be the natural way to deal with the DC–DC converters. Furthermore, the discrete-time model would be preferable in investigation of bifurcations in power electronic systems because it is more accurate than other modeling strategies in predicting various nonlinear phenomena.

The purpose of this paper is to offer a perspective of the study of nonlinear dynamics and bifurcations in voltage-controlled single ended primary inductor DC–DC converters, and to give a useful method for practical considerations in designing. We demonstrate that complex dynamic behaviour is possible under a broad range of parameter values. In particular, we show that the model exhibits not only stable state and low-frequency oscillations, but also the most striking behaviour: intermittency. The paper is organized as follows. Section 2 outlines the operation of the system and derives a nonlinear discrete map. In Section 3, the discrete map is used to study and analyse low-frequency instabilities and intermittent quasi-periodicity through numerical simulations. In Section 4, we analyse these nonlinear phenomena and arrive at some instructive conclusions, which are useful to the further research in this field. Finally, we show some experimental results to verify our findings from simulations.

2. Modeling of SEPICs

2.1. Operating principle

Figure 1 shows the SEPI DC–DC converter with a PWM voltage feedback regulation. Here, both switch and diode are assumed to be ideal, and parasitic elements such as the equivalent-series-resistance (ESR) of inductors, are included in the circuit. To improve the quality and for meeting with some regulation requirements, an active low-pass filter[26] is inserted in the controller which is commonly used in industrial applications. Then, the system in this case is five-dimensional. The output voltage v_2 is the final control target, and the control is achieved by comparing the error signal v_e with an independent sawtooth ramp voltage V_{ramp}. The ramp signal is given by $V_{ramp} = V_L + (V_U - V_L)[(t/T_s) \bmod 1]$, where V_L and V_U are the lower and upper voltage limits of V_{ramp}, and T_s is the switching period.

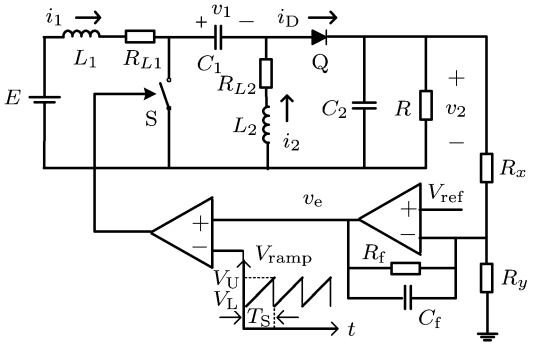


Fig. 1. Schematics of SEPIC with voltage-controlled loop.

In Fig. 1, there are three possible configurations, depending on the state of the switch S and diode Q. The third configuration, where both S and Q are at their off-state (free wheeling stage), appears only when the sum of two inductor currents i_m ($i_m = i_1 + i_2$) crosses zero. In this case, the system is said to operate in a discontinuous current mode (DCM). Otherwise, if the condition $i_m > 0$ always holds, only the first two configurations exist in a switching period, and the system is said to operate in a continuous current mode (CCM). Generally, the dynamic behaviour in each state of the three configurations is given by a linear time invariant (LTI) equation, which can be described as follows:

$$\dot{x} = \begin{cases} \boldsymbol{A}_1\boldsymbol{x} + \boldsymbol{B}_1 E, \text{ state 1;} \\ \boldsymbol{A}_2\boldsymbol{x} + \boldsymbol{B}_2 E, \text{ state 2;} \\ \boldsymbol{A}_3\boldsymbol{x} + \boldsymbol{B}_3 E, \text{ state 3;} \end{cases} \tag{1}$$

where E is the input voltage, $\boldsymbol{x} = [i_1, i_2, v_1, v_2, v_e]^{\mathrm{T}}$ is the state vector of the system, and constant matrices are given by

$$\boldsymbol{A}_1 = \begin{bmatrix} -\frac{R_{L1}}{L_1} & 0 & 0 & 0 & 0 \\ 0 & -\frac{R_{L2}}{L_2} & \frac{1}{L_2} & 0 & 0 \\ 0 & -\frac{1}{C_1} & 0 & 0 & 0 \\ 0 & 0 & 0 & -\frac{1}{RC_2} & 0 \\ 0 & 0 & 0 & -\frac{1}{R_x C_f} & -\frac{1}{R_f C_f} \end{bmatrix},$$

$$\boldsymbol{A}_2 = \begin{bmatrix} -\frac{R_{L1}}{L_1} & 0 & -\frac{1}{L_1} & -\frac{1}{L_1} & 0 \\ 0 & -\frac{R_{L2}}{L_2} & 0 & -\frac{1}{L_2} & 0 \\ \frac{1}{C_1} & 0 & 0 & 0 & 0 \\ \frac{1}{C_2} & \frac{1}{C_2} & 0 & -\frac{1}{RC_2} & 0 \\ 0 & 0 & 0 & -\frac{1}{R_x C_f} & -\frac{1}{R_f C_f} \end{bmatrix},$$

$$\boldsymbol{A}_3 = \begin{bmatrix} 0 & 0 & 0 & 0 & 0 \\ 0 & 0 & 0 & 0 & 0 \\ \frac{1}{C_1} & 0 & 0 & 0 & 0 \\ 0 & 0 & 0 & -\frac{1}{RC_2} & 0 \\ 0 & 0 & 0 & -\frac{1}{R_x C_f} & -\frac{1}{R_f C_f} \end{bmatrix},$$

$$\boldsymbol{B}_1 = \boldsymbol{B}_2 = \begin{bmatrix} \frac{1}{L_1} & 0 & 0 & 0 & a \end{bmatrix}^{\mathrm{T}}$$

and

$$\boldsymbol{B}_3 = \begin{bmatrix} 0 & 0 & 0 & 0 & a \end{bmatrix}^{\mathrm{T}}$$

with $a = \frac{1}{C_f}\left(\frac{1}{R_x} + \frac{1}{R_y} + \frac{1}{R_f}\right)V_{\mathrm{ref}}$.

2.2. Derivation of stroboscopic map

Now, we assume that the converter works in DCM and we begin our research with a suitable discrete-time model. Let $\boldsymbol{x}$ be the state vector as defined previously and further let d be the duty radio of the converter. During each state, the subsystem trajectory can be expressed in closed form and the solution of the subsystem can be written as $\boldsymbol{x}(t) = \mathrm{e}^{\boldsymbol{A}(t-t_0)}\boldsymbol{x}(t_0) + \int_{t_0}^{t} \mathrm{e}^{\boldsymbol{A}(t-\tau)}\boldsymbol{B}u(\tau)\mathrm{d}\tau$. Using the notations $\boldsymbol{x}_n = \boldsymbol{x}(nT_s)$, $\boldsymbol{x}_{n+1} = \boldsymbol{x}((n+1)T_s)$, and applying the technique of successive substitution to the exact state equations (1), we derive the stroboscopic map of the system operating in DCM as follows:

$$\begin{aligned} \boldsymbol{x}_{n+1} = f(\boldsymbol{x}_n, t_{1,n}, t_{2,n}) &= \boldsymbol{\Phi}_3(T_s - t_{1,n} - t_{2,n}) \\ &\times \boldsymbol{\Phi}_2(t_{2,n})\boldsymbol{\Phi}_1(t_{1,n})(\boldsymbol{x}_n + \boldsymbol{\psi}_1(t_{1,n})E) \\ &+ [\boldsymbol{\Phi}_3(T_s - t_{1,n} - t_{2,n})\boldsymbol{\Phi}_2(t_{2,n})\boldsymbol{\psi}_2(t_{2,n}) \\ &+ \boldsymbol{\Phi}_3(T_s - t_{1,n} - t_{2,n})\boldsymbol{\psi}_3(T_s - t_{1,n} - t_{2,n})]E, \end{aligned} \tag{2}$$

where subscript n denotes the value at the beginning of the n-th switching period, $t_{1,n} = \mathrm{d}T_s$ is the time duration when the switch is held closed and the diode is reverse-biased, $t_{2,n}$ is the time duration when the switch is turned off and the diode is forward-biased, $\boldsymbol{\Phi}_i(\xi) = \mathrm{e}^{\boldsymbol{A}_i\xi}$, $\boldsymbol{\psi}_i(\xi) = [\boldsymbol{\Phi}_i(\xi) - \boldsymbol{I}]\boldsymbol{A}_i^{-1}\boldsymbol{B}_i$, $i = 1, 2, 3$. In order to obtain the solution of the stroboscopic map (2), $t_{1,n}$ must be obtained.

Thus, our next step is to find the feedback equation that connects $t_{1,n}$ to $\boldsymbol{x}$. To find the defining equation for $t_{1,n}$, we note that the converter switches from state 1 to 2 whenever $v_e = V_{\mathrm{ramp}}$ within a pulse clock period. The error signal v_e can be derived from the corresponding sub-equation in Eq. (1)

$$v_e = a\tau - \frac{\tau\tau_1 \mathrm{e}^{-\omega t}}{1 - \omega\tau} + (v_{e,n} - a\tau - \frac{\tau\tau_1}{1 - \omega\tau})\mathrm{e}^{-t/\tau}, \tag{3}$$

where $\tau = R_f C_f$, $\tau_1 = v_{2,n}/R_x C_f$, $\omega = 1/RC_2$, $v_{2,n}$ and $v_{e,n}$ indicate the sampling values of v_2 and v_e at $t = nT_s$, respectively. For brevity, we introduce the notation $\sigma = v_e - V_{\mathrm{ramp}}$. So, the switching function can be written as

$$\begin{aligned} \sigma(\boldsymbol{x}_n, t_{1,n}) = a\tau &- \frac{\tau\tau_1 \mathrm{e}^{-\omega t_{1,n}}}{1 - \omega\tau} \\ &+ \left(v_{e,n} - a\tau - \frac{\tau\tau_1}{1 - \omega\tau}\right)\mathrm{e}^{-t_{1,n}/\tau} \\ &- \left[V_L + V_M\left(\frac{t_{1,n}}{T_s} \bmod 1\right)\right]. \end{aligned} \tag{4}$$

Hence, we know that the dynamics of the system in each period are equivalent to that on a switching surface which is time-dependent. Note that the switching instants $t_{1,n}$ are naturally, the solutions of transcendental equation (4) and therefore are usually given numerically, i.e., by Newton–Raphson method.[27]

3. Simulation results and analysis

Previous studies on voltage-controlled SEPICs have mainly focused on the steady-state design and control aspects. The detailed dynamics have seldom

been investigated. Here, we will show that the values of the feedback gain K ($K = R_{\rm f}/R_x$) seriously influence the dynamics of the SEPIC. The numerical simulations are performed with the following parameter values: $E = 10$ V, $L_1 = L_2 = 600$ μH, $R_{L1} = R_{L2} = 0.001$ Ω, $C_1 = 4.7$ μF, $C_2 = 47$ μF, $V_{\rm ref} = 3.5$ V, $V_{\rm L} = 3$ V, $V_{\rm U} = 8$ V, $C_{\rm f} = 0.01$ μF, switching frequency $f_{\rm s} = 10$ kHz, and feedback sensor gain $R_y/(R_x + R_y) = 3/25$.

We now begin with a series of computer simulations to make an initial evaluation of the possible bifurcation phenomena. To mimic the true behaviours of the circuit, the exact state equations (1) are used for simulation. Moreover, we restrict our attention to the case when K is the control variable, while the other parameters are treated as circuit parameters. Essentially, for each set of parameters, cycle-by-cycle time-domain waveforms are generated by solving the appropriate linear equation in a sub-interval of time, according to different switching states. After the transient process, we capture the steady-state time-domain waveforms of the system. Since the current $i_{\rm m}$ depicts the operating mode of the system, we will pay more attention to the time-domain waveforms of $i_{\rm m}$. Moreover, the phase portrait is constructed between $i_{\rm m}$ and v_2 to explain the stability from the nonlinear viewpoint.

3.1. Neimark–Sacker bifurcation

With the feedback gain K as the bifurcation parameter ranging from 0.1 to 0.18, and taking the initial conditions (0.6, 1, 10, 10, 0), the following bifurcation diagrams, time domain waveforms, trajectories in the phase plane (v_2, $i_{\rm m}$), and the corresponding Poincaré sections[13] illustrate the main results concerning the steady-state behaviour of the system.

In Fig. 2, typical bifurcation diagrams for the output voltage and duty ratio are illustrated, which exhibit the view of the parameter evolvement process. The corresponding nonlinear phenomena can be observed from Fig. 3 to Fig. 5, described as follows. When K is relatively small, i.e., $K = 0.1136$, the system operates in a stable period-1 condition. Figures 3(a) and 3(b) show the time domain waveforms of $i_{\rm m}$ and the corresponding stroboscopic sampling values, respectively. Moreover, the trajectory spirals into a fixed period-1 orbit and its Poincaré section is characterized by one dot, as shown in Figs. 3(c) and 3(d), respectively. From Fig. 3, we see clearly that the converter works in CCM ($i_{\rm m} > 0$). When we further increase K, the system exhibits a high periodic state, with small amplitude of low-frequency oscillation. As shown in Fig. 4, when K is adjusted to 0.1250, the low-frequency oscillation begins to develop with very small amplitude of $i_{\rm m}$ (about 0.04 A). Figure 4(a) shows the time-domain waveforms of $i_{\rm m}$. The stroboscopic sampling values of $i_{\rm m}$ is presented in Fig. 4(b) from which we can observe that $i_{\rm m} > 0$ always holds all the time. Figures 4(c) and 4(d) show the trajectory and its Poincaré section, which indicate the period-11 state. It is relevant to point out that the system may exhibit different periodic states, i.e., period-29, period-13, period-31 and period-14, etc., with different values of K when K lies in the region (0.125, 0.129). The occurrence of these high periodic states could not be explained by period-adding sequence[13] which is well known to occur in low-order DC–DC converters when low-frequency instability takes place. By increasing K further, i.e., K=0.1318, the low-frequency oscillation becomes quite serious. In Figs. 5(a) and 5(b), we can see that the system oscillates with a very large amplitude. In this case, a quasi-periodic orbit can be observed; its trajectory is characterized by a 2D torus as shown in Figs. 5(c) and 5(d). From Fig. 5, we find that the trajectory of the Poincaré section is an invariant closed curve that emerges from the fixed point of the map; and the conduction mode changes from CCM under the originally stable period-1 and high periodic states, to the intermittent changes between CCM and DCM operation modes. From the nonlinear viewpoint, the occurrence of the low-frequency quasi-periodic orbit reflects that the system undergoes a Neimark–Sacker bifurcation.[13] From a physical point of view the system behaviour is therefore characterized by the existence of two different incommensurate frequencies. One is the switching frequency while the other is related to the circuit parameters, which can be derived by computing characteristic multipliers of the system when the Neimark–Sacker bifurcation occurs.[28] When we increase K yet further, the system may settle in a quasi-periodic orbit or higher periodic orbit (phase-locking).

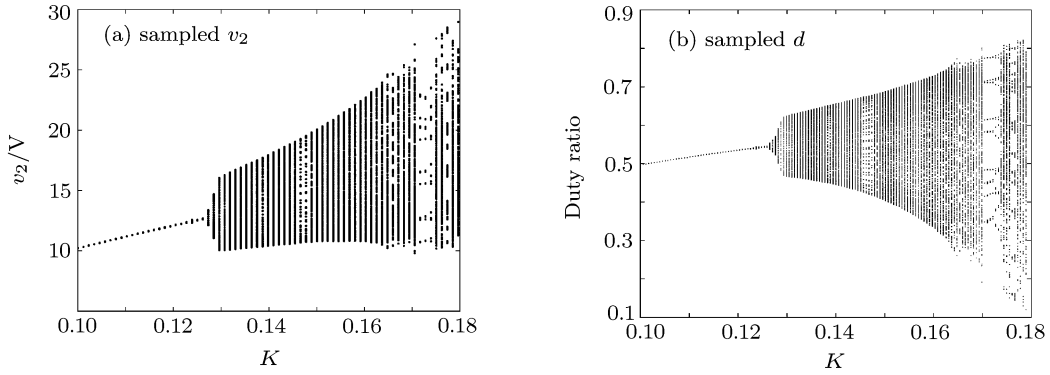


Fig. 2. Bifurcation diagrams for $0.1 < K < 0.18$.

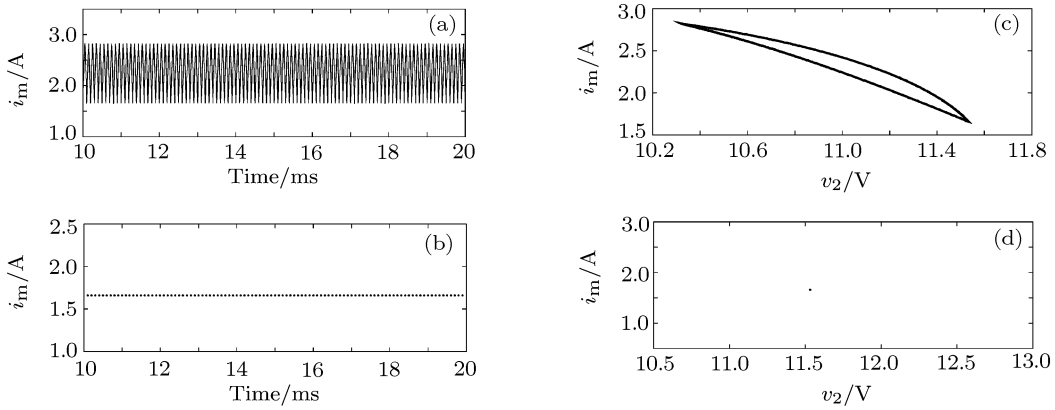


Fig. 3. Stable period-1 orbit ($K = 0.1136$). (a) Time domain waveforms of i_m; (b) stroboscopic sampling values of i_m; (c) phase-space trajectory; (d) Poincaré section.

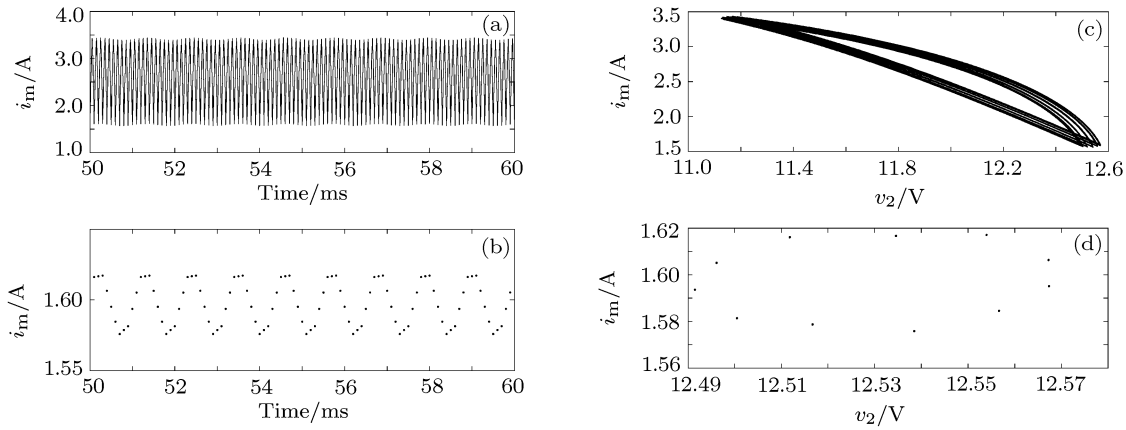


Fig. 4. Period-11 orbit ($K = 0.1250$). (a) Time domain waveforms of i_m; (b) stroboscopic sampling values of i_m; (c) phase-space trajectory; (d) Poincaré section.

From the above simulation results, we know that as the feedback gain K increases, the SEPIC under study undergoes a low-frequency bifurcation (Neimark–Sacker bifurcation) and settles in a quasi-periodic orbit or higher periodic orbit. It is shown that the conduction mode will change from CCM under the originally stable period-1 and high periodic states to the intermittent switchings between CCM and DCM. Thus, we conjecture that the DCM operating mode may be responsible to the formation of the 2D torus. Moreover, since the trajectory of the Poincaré section at $K = 0.1318$ exhibits a limit cycle, there exist no other limit cycles. This fact is ensured by the characteristics of the limit cycle, and can be used to explain the occurrence of the phase-locking periodic orbits in the neighbourhood of $K = 0.1318$. Furthermore, the Poincaré section of the 2D

torus is born with nonnull amplitude, so the Neimark–Sacker bifurcation is called subcritical or abnormal.[29] In Ref. [30], the authors reported that in the voltage-controlled Boost the conduction mode border may be related to the period-1 region bifurcation, which means the change of conduction mode takes place before the bifurcation of the period-1 region. However, in the SEPIC under study, the conduction mode border is not inside the period-1 region.

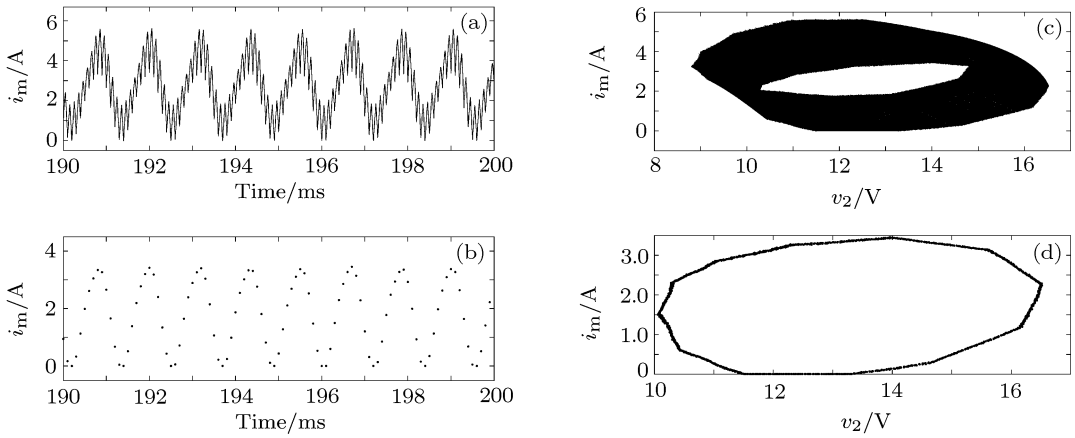


Fig. 5. Quasi-periodicity orbit ($K = 0.1318$). (a) Time domain waveforms of i_m; (b) stroboscopic sampling values of i_m; (c) phase-space trajectory; (d) Poincaré section.

3.2. Intermittent quasi-periodic bifurcation

Now, we will show that when the feedback gain decreases to a relatively small value, the system may suffer from a new kind of bifurcation.

We start with a relatively low value of K and vary it. The corresponding bifurcation diagrams for v_2 are shown in Fig. 6. Figure 6(a) is the bifurcation diagram when K is varied in the range (0.03, 0.04). In order to see the details more clearly, partially enlarged diagrams in the ranges (0.0332, 0.0345) and (0.0386, 0.04) are given in Figs. 6(b) and 6(c), respectively. From Fig. 6, we see that a period-1 state bifurcates suddenly into a quasi-periodic attractor when K increases to 0.0332, and the state maintains until $K = 0.0345$. Then, the quasi-periodic state vanishes suddenly, and the system returns to a regular period-1 state again. It is very interesting that when K increases to 0.0386, the quasi-periodic state comes forth again. Subsequently, quasi-periodic and period-1 state occurs alternately (Fig. 6(c)). This suggests that the behaviour differs from the well-known quasi-periodic bifurcation. So, we call this phenomenon 'intermittent quasi-periodic bifurcation'. The typical time domain waveforms, trajectories in the phase plane (v_2, i_m), and the corresponding Poincaré sections are shown in Figs. 7 and 8. As K increases further, the intermittent quasi-periodic oscallision ends abruptly at a certain critical value, and the period-1 state occurs and lasts for a broad range of parameter value.

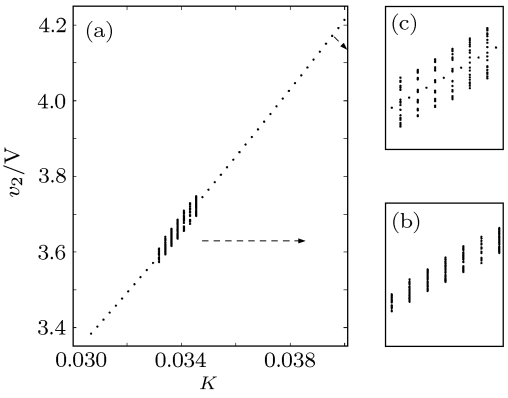


Fig. 6. Bifurcation diagrams for $0.03 < K < 0.04$. (a) Bifurcation diagram for $0.03 < K < 0.04$; (b) partially enlarged bifurcation diagram for $0.0332 < K < 0.0345$; (c) partially enlarged bifurcation diagram for $0.0386 < K < 0.04$.

Comparing Fig. 8 with Fig. 5, we see clearly that the oscillating frequency tends to be considerably high when the intermittent quasi-periodic bifurcation emerges. Interestingly, in spite of the instability of these orbits, the converter still behaves properly and the output voltage ripple is small.

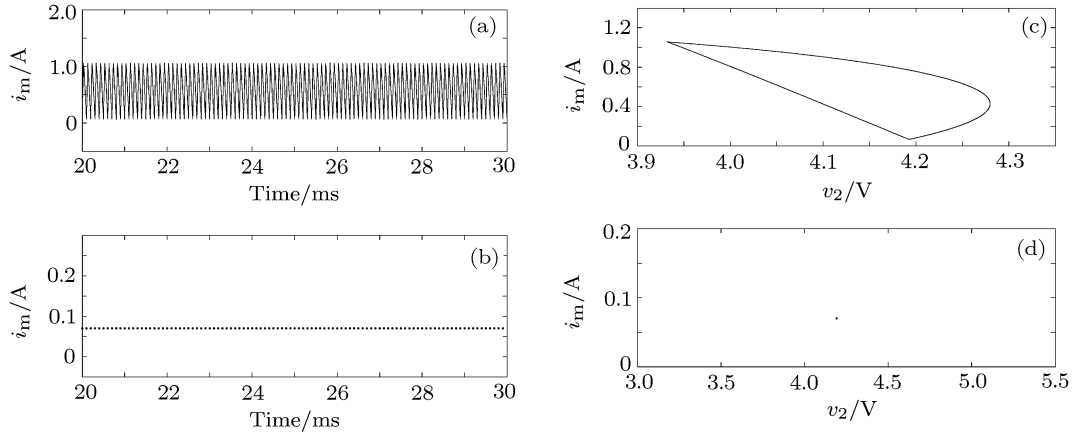


Fig. 7. Stable period-1 orbit ($K = 0.03864$). (a) Time domain waveforms of i_m; (b) stroboscopic sampling values of i_m; (c) phase-space trajectory; (d) Poincaré section.

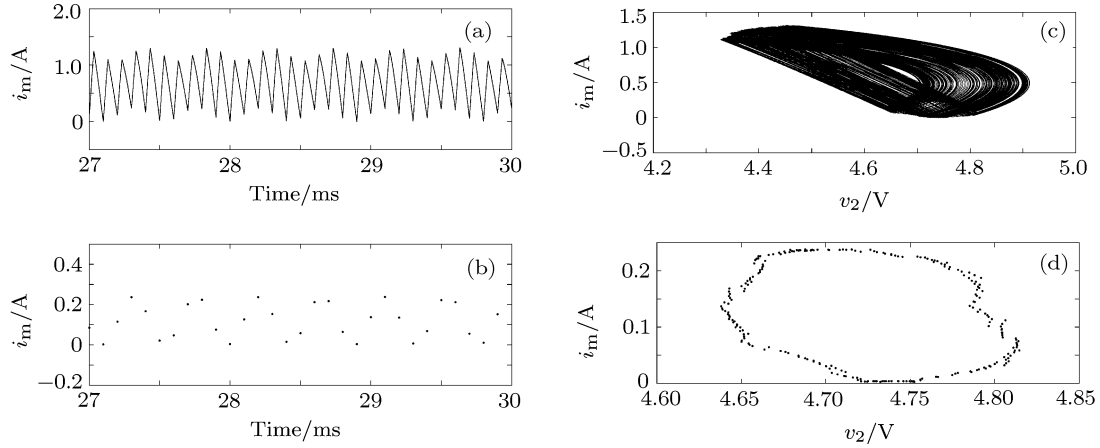


Fig. 8. Quasi-periodic orbit ($K = 0.03989$). (a) Time domain waveforms of i_m; (b) stroboscopic sampling values of i_m; (c) phase-space trajectory; (d) Poincaré section.

4. Analysis of bifurcation behaviours

In this section, we show that the unusual type of quasi-periodic behaviour described above is due to the occurrence of a Neimark–Sacker bifurcation, rather than the transient chaos described in Ref. [31]. From Figs. 6–8, we know that the system works in CCM operation mode all the time before the occurence of the quasi-periodic orbits. Henceforth, we start our theoretical analysis with Jacobian matrix of the stroboscopic map,

$$\boldsymbol{x}_{n+1} = f(\boldsymbol{x}_n, t_{1,n}) = \boldsymbol{\Phi}_2(t_{2,n})\boldsymbol{\Phi}_1(t_{1,n})\boldsymbol{x}_n + [\boldsymbol{\Phi}_2(t_{2,n})\boldsymbol{\psi}_1(t_{1,n}) + \boldsymbol{\psi}_2(t_{2,n})]E, \tag{5}$$

where the converter works in CCM, $t_{2,n} = T_s - t_{1,n}$. The analysis method of Jacobian matrix plays an important role in the study on dynamical systems, and the essence of using Jacobian matrix in the analysis of the dynamical systems lies in the capture of the dynamics in the small neighbourhood of the system's equilibrium point.

The equilibrium point $\boldsymbol{x}^*$ of the stroboscopic map (5) can be obtained by enforcing periodicity: $\boldsymbol{x}_n = f(\boldsymbol{x}_n, t_n)$. By doing so and using Eq. (5) we obtain

$$\boldsymbol{x}^* = (\boldsymbol{I} - \boldsymbol{\Phi}_2(t^*_{2,n})\boldsymbol{\Phi}_1(t^*_{1,n}))^{-1}(\boldsymbol{\Phi}_2(t^*_{2,n})[\boldsymbol{\psi}_1(t^*_{1,n}) + \boldsymbol{\psi}_2(t^*_{2,n})]E. \tag{6}$$

From Eqs. (4) and (5), we can derive the Jacobian matrix at the equilibrium point $\boldsymbol{x}^*$,

$$\boldsymbol{J}(\boldsymbol{x}^*) = \frac{\mathrm{d}f}{\mathrm{d}\boldsymbol{x}_n}\Big|_{\boldsymbol{x}_n = \boldsymbol{x}^*} = \frac{\partial f}{\partial \boldsymbol{x}_n} - \frac{\partial f}{\partial t_{1,n}}\left(\frac{\partial \sigma}{\partial t_{1,n}}\right)^{-1}\frac{\partial \sigma}{\partial \boldsymbol{x}_n}, \tag{7}$$

where

$$\frac{\partial f}{\partial \boldsymbol{x}_n} = \boldsymbol{\Phi}_2(t^*_{2,n})\,\boldsymbol{\Phi}_1(t^*_{1,n}),$$
$$\frac{\partial f}{\partial t_n} = (\boldsymbol{A}_1 - \boldsymbol{A}_2)\,\boldsymbol{\Phi}_2(t^*_{2,n})\,\boldsymbol{\Phi}_1(t^*_{1,n})\boldsymbol{x}_n + [-\boldsymbol{A}_2\,\boldsymbol{\Phi}_2(t^*_{2,n})\boldsymbol{\psi}_1(t^*_{1,n}) + \boldsymbol{\Phi}_2(t^*_{2,n})\,\boldsymbol{\Phi}_1(t^*_{1,n})\boldsymbol{B}_1 - \boldsymbol{\Phi}_2(t^*_{2,n})\boldsymbol{B}_2]E,$$
$$\frac{\partial \sigma}{\partial t_n} = \frac{\omega\tau\tau_1 \mathrm{e}^{-\omega t_{1,n}}}{1-\omega\tau} - \left(\frac{v_{\mathrm{e},n}}{\tau} - a + \frac{\tau_1}{1-\omega\tau}\right)\mathrm{e}^{-t_{1,n}/\tau} - \frac{V_{\mathrm{M}}}{T_{\mathrm{s}}},$$
$$\frac{\partial \sigma}{\partial \boldsymbol{x}_n} = \left[0,\ 0,\ 0, \frac{\tau}{R_x C_{\mathrm{f}}(1-\omega\tau)}(\mathrm{e}^{-t_{1,n}/\tau} - \mathrm{e}^{-\omega t_{1,n}}),\ \mathrm{e}^{-t_{1,n}/\tau}\right].$$

Therefore, the characteristic multipliers of the system satisfy

$$\det[\lambda I - \boldsymbol{J}(\boldsymbol{x}^*)] = 0, \tag{8}$$

where $\boldsymbol{I}$ is the unit matrix. The equilibrium point λ and the periodic orbit are asymptotically stable if and only if all characteristic multipliers λ lie inside the unit circle. Any crossing from the interior of the unit circle to the exterior indicates a bifurcation. For an n-dimensional discrete-time map, whatever bifurcations occur, we have $|\lambda_i| = 1$ $(i \in n)$ at the bifurcating point. So, we can write $\lambda_i = \mathrm{e}^{\mathrm{i}\,\theta}$. For $\theta = 0$, saddle node bifurcation takes place, while for $\theta = \pi$, period-doubling bifurcation can occur. For other values of θ, a Neimark–Sacker bifurcation is possible. Essentially, using Eqs. (6)–(8), we can locate the onset of bifurcation in the system involved.

Here, we are mainly interested in the loci where K varies slowly in the ranges (0.0332, 0.0345) and (0.0386, 0.04). The results are based on the same set of parameter values as those used for generating Fig. 6. To maintain conciseness, we exemplify here the typical loci graphically in Fig. 9. We find that a complex conjugate pair of eigenvalues jump continuously out of the unit circle. In Fig. 9(a), $\lambda_{1,2} = 0.4512 \mp \mathrm{i}\,0.9470$, $|\lambda_{1,2}| \approx 1.0490$, while in Fig. 9(b) $\lambda_{1,2} = 0.0981 \mp \mathrm{i}\,0.9959$, $|\lambda_{1,2}| \approx 1.0007$. As stated in Ref. [32], we can conjecture that the system undergoes a Neimark–Sacker bifurcation within the two parameter regions, respectively.

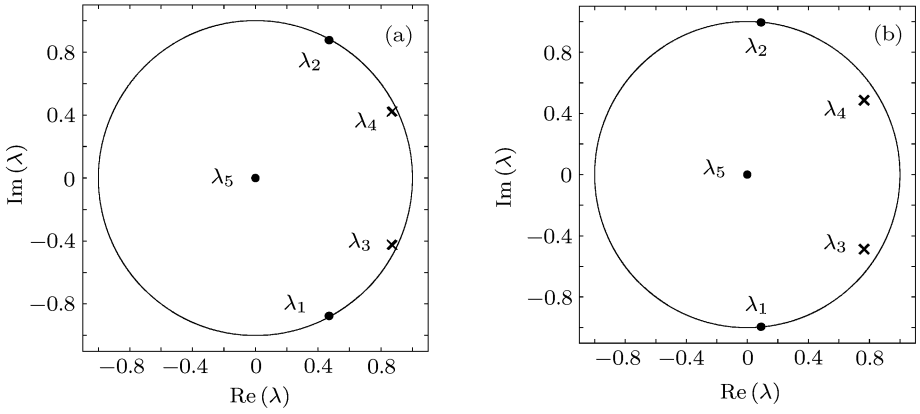


Fig. 9. Loci of characteristic multipliers $\lambda_{1,2}$ as K varies. (a) Results for K near 0.0332; (b) results for K near 0.0386.

5. PSPICE verifications

Let us consider a PSPICE-based circuit as shown in Fig. 10. Figure 11 shows the waveforms for $K = 0.1136$, where the system works in stable operation. Figure 11(a) shows the time-domain waveforms of output voltage v_2 (upper) and current i_{m} (lower), from which we observe that the system works in CCM operation mode. Figure 11(b) shows trajectories in the phase plane (v_2, i_{m}), which indicates a typical period-1 trajectories. Figure 12 shows the waveforms for K=0.1218, where low-frequency instability can be seen clearly. Figure 12(a) shows the time-domain waveforms of output voltage v_2 (upper) and current i_{m} (lower), from which we can see

that the system works in CCM operation mode all the time. Figure 12(b) gives trajectories in the phase plane (v_2, i_m). Figure 13 depicts the waveforms for K=0.1318, where low-frequency instability appears with a larger oscillation amplitude. Figure 13(a) shows the time-domain waveforms of output voltage v_2 (upper) and current i_m (lower), from which we can see that the system operation begins to fluctuate between CCM and DCM. Figure 13(b) illustrates trajectories in the phase plane (v_2, i_m), which is really a 2D torus. Moreover, we also verify the dynamics when K is relatively small, i.e., $K = 0.039$. The results are shown in Fig. 14, which implies a low-frequency quasi-periodic behaviour of the system.

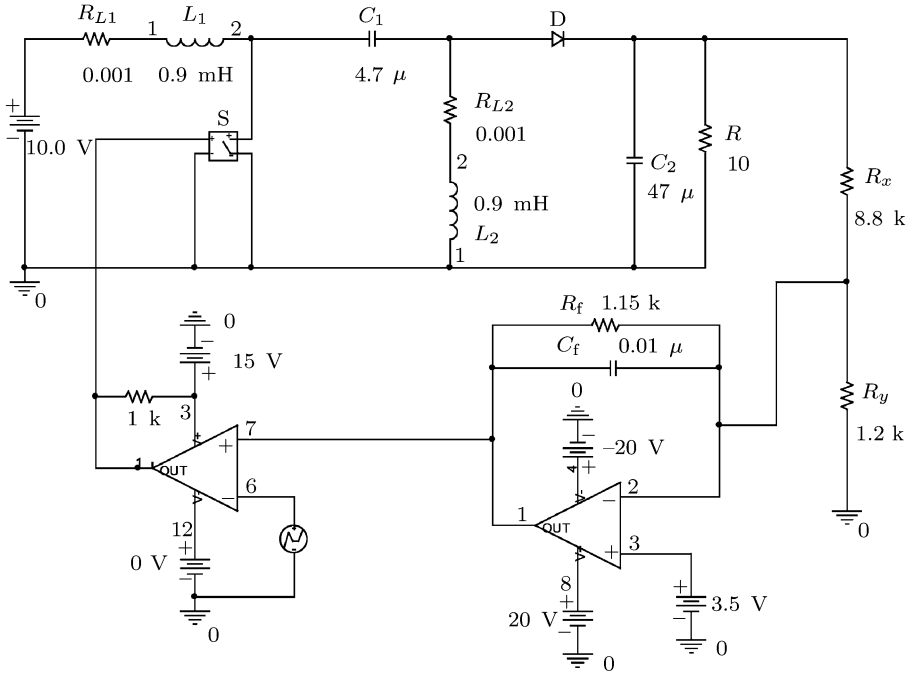


Fig. 10. PSPICE-based circuit.

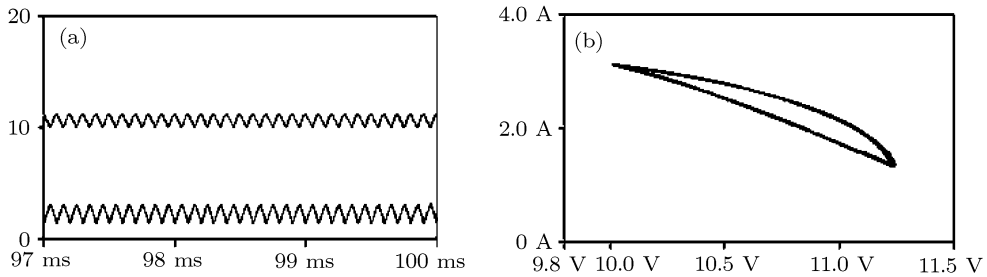


Fig. 11. Stable period-1 orbit ($K = 0.1136$). (a) Time domain waveforms of v_2 (upper) and i_m (lower); (b) phase-space trajectory of (v_2, i_m).

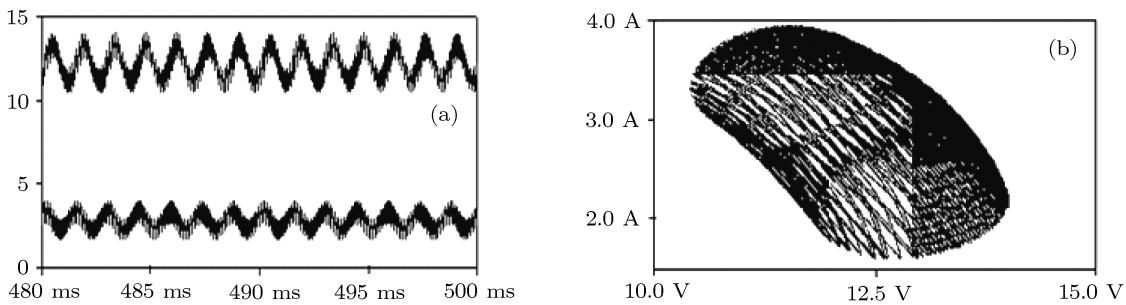


Fig. 12. Low-frequency oscillation under CCM ($K = 0.1218$). (a) Time domain waveforms of v_2 (upper) and i_m (lower); (b) phase-space trajectory of (v_2, i_m).

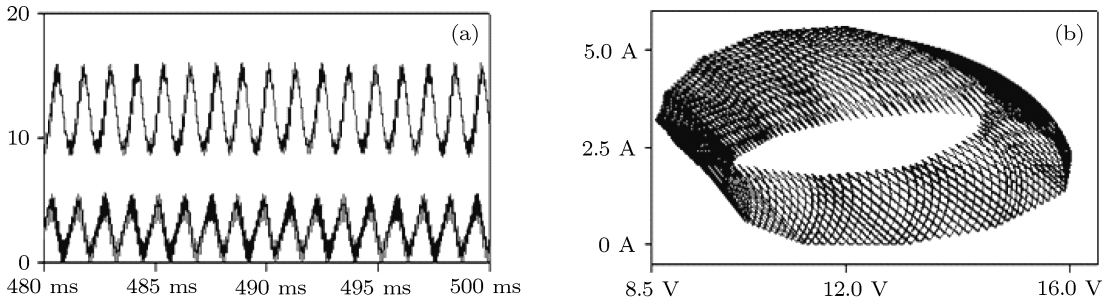


Fig. 13. Quasi-periodic orbit with lower frequency ($K = 0.1318$). (a) Time domain waveforms of v_2 (upper) and $i_{\rm m}$ (lower); (b) phase-space trajectory of (v_2, $i_{\rm m}$).

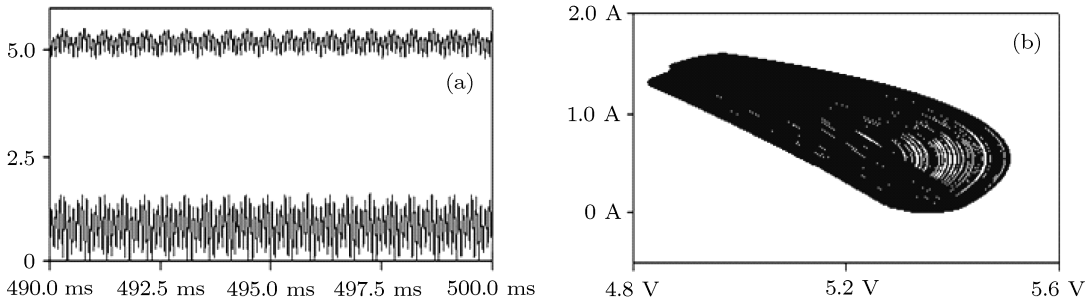


Fig. 14. Quasi-periodic orbit with higher frequency ($K = 0.039$). (a) Time domain waveforms of v_2 (upper) and $i_{\rm m}$ (lower); (b) phase-space trajectory of (v_2, $i_{\rm m}$).

Comparing the results shown in Section 3 and Section 5, we can conclude that they agree very well with each other qualitatively.

6. Conclusion

In this paper, a detailed study on the stability of the voltage-controlled SEPIC has been made. The circuit is designed to operate in CCM, which is extensively used in industrial applications. We have reported the results from exact cycle-by-cycle circuit simulations, theoretical analysis as well as PSPICE verifications, and revealed a new kind of low-frequency instability. We have demonstrated that the model under a broad range of parameter space, exhibits not only stable state and low-frequency oscillations, but also the most striking behaviour: intermittency. Our focus is put on the mechanism of low-frequency oscillations occurring in the converter. It is shown that the system manifests itself as a Neimark–Sacker bifurcation when the intermittent quasi-periodic oscillation comes forth. It is further shown that the operating mode DCM may be responsible for the formation of the 2D torus. Finally, it is necessary to point out that, as the circuit parameters vary, there exist more complicated and diversiform phenomena in the high-order SEPIC than in the low-order regulators.

References

[1] Dai D, Ma X K and Tse C K 2006 *Chin. Phys.* **15** 2535
[2] Bao B C, Liu Z and Xu J P 2009 *Acta Phys. Sin.* **58** 2949 (in Chinese)
[3] Qiu D Y, Yang R and Zhang B 2008 *Acta Phys. Sin.* **57** 1389 (in Chinese)
[4] Zou Y L, Luo X S and Chen G R 2006 *Chin. Phys.* **15** 1719
[5] Lu W G, Zhou L W, Luo Q M and Du X 2007 *Acta Phys. Sin.* **56** 6275 (in Chinese)
[6] Zhao Y B, Zhang D Y and Zhang C J 2007 *Chin. Phys.* **16** 933
[7] Ren H P and Liu D 2005 *Chin. Phys.* **14** 1352
[8] Zhou Y F, Tse C K, Qiu S S and Chen J N 2005 *Chin. Phys.* **14** 61
[9] Banerjee S 1997 *IEEE Trans. Circ. Syst.* I **44** 847
[10] Hamill D C and Jeffries D J 1988 *IEEE Trans. Circ. Syst.* **35** 1059
[11] Deane J H B and Hamill D C 1990 *IEEE Trans. Power Electronics* **5** 260
[12] Deane J H B 1992 *IEEE Trans. Circ. Syst.* I **39** 680

[13] Aroudi A E, Benadero L, Toribio E and Olivar G 1999 *IEEE Trans. Circ. Syst.* I **46** 1374
[14] Zhusubaliyev Z T, Soukhoterin E A and Mosekilde E 2003 *IEEE Trans. Circ. Syst.* I **50** 1047
[15] Mazumder S K, Nayfeh A H and Boroyevich D 2001 *IEEE Trans. Power Electronics* **16** 201
[16] Johnson M J 1993 *IEEE APEC* p. 207
[17] Gu W 2005 *IEEE APEC* p. 906
[18] Liu F 2008 *Chin. Phys.* B **17** 2394
[19] Mohamed B D, Aroudi A E, Roberto G and Martinez-Salamero L 2002 *IEEE ICIT* p. 1055
[20] Liu F, Zhang H and Ma X K 2007 *Trans. Chin. Electrotechnical Soc.* **22** 86 (in Chinese)
[21] Wang S, Zhou Y, Iu H H C and Chen J 2007 *IEEE ISCAS* p. 2407
[22] Alfayyoumi M, Nayfeh A H and Borojevic D 2000 *Int. J. Bifur. Chaos* **10** 373
[23] D'Amico M B, Moiola J L and Paolini E E 2004 *Circ. Syst. Sig. Processing* **23** 517
[24] Vorperian V 1990 *IEEE Trans. Aerospace and Electronic Syst.* **26** 497
[25] Middlebrook R D and Cuk S 1977 *Int. J. Electronics* **42** 521
[26] Tse K K and Chung H S 1998 *IEEE Trans. Power Electronics* **13** 222
[27] Parker T S and Chua L O 1989 *Practical Numerical Algorithms for Chaotic Systems* (New York: Springer-Verlag) p. 121
[28] Aroudi A E, Debbat M, Giral R, Olivar G, Benadero L and Toribio E 2005 *Int. J. Bifur. Chaos* **15** 1549
[29] Aroudi A E and Leyva L 2001 *IEEE Trans. Circ. Syst.* I **48** 967
[30] Toribio E, Aroudi A E, Olivar G and Benadero L 2000 *IEEE Trans. Power Electronics* **15** 1163
[31] Gavrilets S and Hastings A 1995 *Proceedings: Biological Sciences* **261** 233
[32] Zhusubaliyev Z T and Mosekilde E 2006 *IEEE Trans. Circ. Syst.* I **53** 1839